

# Complex Inverse Design of Meta-optics by Segmented Hierarchical Evolutionary Algorithm

Zhongwei Jin,<sup>†,●</sup> Shengtao Mei,<sup>†,●</sup> Shuqing Chen,<sup>‡,●</sup> Ying Li,<sup>‡,●</sup> Chen Zhang,<sup>§</sup> Yanliang He,<sup>‡</sup> Xia Yu,<sup>†</sup> Changyuan Yu,<sup>†,||</sup> Joel K. W. Yang,<sup>¶,#,○</sup> Boris Luk'yanchuk,<sup>¶,△</sup> Shumin Xiao,<sup>\*,§,○</sup> and Cheng-Wei Qiu<sup>\*,†,▲,○</sup>

<sup>†</sup>Department of Electrical and Computer Engineering, National University of Singapore, 4 Engineering Drive 3, Singapore 117583

<sup>‡</sup>International Collaborative Laboratory of 2D Materials for Optoelectronics Science and Technology, Shenzhen University, Nanhai Avenue 3688, Shenzhen, Guangdong 518060, People's Republic of China

<sup>§</sup>State Key Laboratory on Tunable Laser Technology, Ministry of Industry and Information Technology Key Lab of Micro-Nano Optoelectronic Information System, Shenzhen Graduate School, Harbin Institute of Technology, Shenzhen, Guangdong 518055, People's Republic of China

<sup>||</sup>Department of Electronic and Information Engineering, The Hong Kong Polytechnic University, Hung Hom, Kowloon, Hong Kong

<sup>¶</sup>Singapore University of Technology and Design, 8 Somapah Road, Singapore 487372

<sup>#</sup>Institute of Materials Research and Engineering, A\*STAR (Agency for Science, Technology and Research), 2 Fusionopolis Way, #08-03 Innovis, Singapore 138634

<sup>▲</sup>Division of Physics and Applied Physics, School of Physical and Mathematical Sciences, Nanyang Technological University, Singapore 637371

<sup>△</sup>Faculty of Physics, Lomonosov Moscow State University, Moscow 119991, Russia

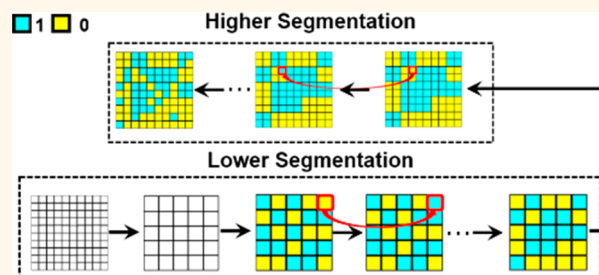
<sup>○</sup>SZU-NUS Collaborative Innovation Center for Optoelectronic Science and Technology, Shenzhen University, Shenzhen 518060, People's Republic of China

## Supporting Information

**ABSTRACT:** With the recent burgeoning advances in nanooptics, ultracompact, miniaturized photonic devices with high-quality and spectacular functionalities are highly desired. Such devices' design paradigms often call for the solution of a complex inverse nonanalytical/semianalytical problem. However, currently reported strategies dealing with amplitude-controlled meta-optics devices achieved limited functionalities mainly due to restricted search space and demanding computational schemes. Here, we established a segmented hierarchical evolutionary algorithm, aiming to solve large-pixelated, complex inverse meta-optics design and fully demonstrate the

targeted performance. This paradigm allows significantly extended search space at a rapid converging speed. As typical complex proof-of-concept examples, large-pixelated meta-holograms are chosen to demonstrate the validity of our design paradigm. An improved fitness function is proposed to reinforce the performance balance among image pixels, so that the image quality is improved and computing speed is further accelerated. Broadband and full-color meta-holograms with high image fidelities using binary amplitude control are demonstrated experimentally. Our work may find important applications in the advanced design of future nanoscale high-quality optical devices.

**KEYWORDS:** *meta-optics, complex large-pixelated inverse design, fast-converging algorithm, segmented hierarchical evolutionary algorithm, full-color meta-holograms*



The ultracompact size and ability of arbitrarily controlling light's phase,<sup>1–4</sup> amplitude,<sup>5–8</sup> and polarization status<sup>9–12</sup> with metasurfaces has attracted

Received: October 31, 2018

Accepted: January 2, 2019

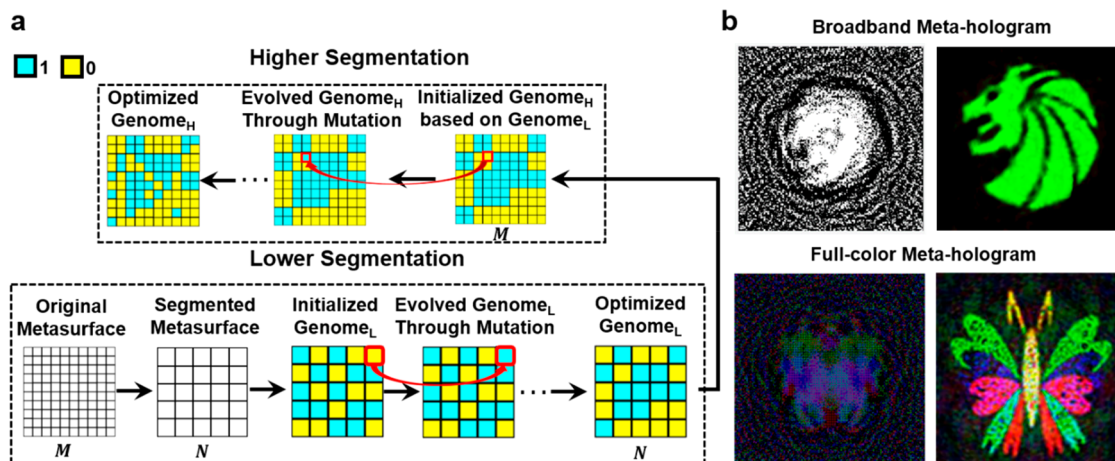


**Figure 1.** Segmented hierarchical evolutionary algorithm (SHEA) can be employed for various complex large-pixelated inverse design. (a) Scheme of SHEA. The cyan and yellow blocks represent pixel states denoted as value “1” and “0”, respectively. (b) Two exemplified patterns for large-pixelated broadband meta-hologram and full-color meta-hologram. Emblem used with permission from Seven Lions Music LLC.

researchers from different fields to design meta-optics devices according to specific requirements. The Gerchberg–Saxton (GS) algorithm<sup>13,14</sup> is widely used to connect the phase distribution of meta-optics design with its far-field diffraction pattern. However, algorithms that link the amplitude distribution of optical elements with their near-field/far-field optical responses are far from satisfactory on both requirements of search space and computing power. As a matter of fact, amplitude-controlled photonic elements can find more applications where phase-controlled photonic elements may not be able to realize. So far, phase-controlled meta-optics have been mainly explored for out-of-plane photonic elements (light penetrates through meta-devices from one side to the other side). However, amplitude-controlled meta-optics can be applied not only for out-of-plane photonic elements but also for in-plane photonic devices (light propagates along the surface of meta-device, e.g., surface wave or confined-mode wave) such as the wavelength multiplexer<sup>15,16</sup> for functional waveguide design. Meanwhile, the amplitude-controlled design strategy can also be employed in the optimization of nanostructures according to different needs.<sup>17,18</sup> Genetic algorithm (GA, also named evolutionary algorithm<sup>7</sup>) and modified GA (also named direct-binary search<sup>15</sup>) are two of the most frequently used strategies in these situations. In GA, populations are evolved through selection, crossover, and mutation, and finally only the genome (a serial of chromosomes arranged in a certain sequence) which can provide the best behavior among the populations will be left, thus providing the optimized result.<sup>19</sup> So far, GA has been widely employed in electromagnetic study for inverse meta-optics designs,<sup>20–22</sup> from integrated optical components, such as optical waveguides<sup>15</sup> and beam splitters,<sup>21</sup> to flat optical devices, for example, flat lens<sup>7</sup> and simple holograms.<sup>8,22</sup> Apart from these, the morphologies of nanostructures can also be tailored toward specific requirements, such as larger field enhancement<sup>23</sup> or higher scattering efficiency<sup>17</sup> through coupling the algorithm with appropriate analytical models. However, in the visible optical frequency range, if complex functionalities are needed, the search space of parameters should be very large, leading to extremely long length of genome in GA, thus requiring a high demand for computational load and computing time. Compared with GA, the

modified GA is a relatively “clumsy” approach which searches for the optimized solution by changing the state of the elements of an initially generated genome one by one in a random sequence. The mutation-only evolutionary process in modified GA can force the genome to converge on the target monotonously, and it requires much less computational load.<sup>24</sup> However, when the search space is large, the converging time of modified GA is still relatively long and the converging ability is sometimes limited. In this work, we propose a **segmented hierarchical evolutionary algorithm (SHEA)** which can solve large-pixelated inverse meta-optics design problems. Through coupling with appropriate theoretical models, such a design paradigm can be applied for various meta-optics devices with complex functionalities. As typical proof-of-concept examples, complex meta-holograms are designed and experimentally demonstrated.

## RESULTS

Suppose there are  $M \times M$  pixels arranged on the metasurface, as shown in Figure 1a. Here, an  $M \times M$  array represents the state of each pixel. If the pixel’s state is chosen to be “1”, light coming through the pixel will contribute to the far-field diffraction pattern of the optical device; on the contrary, if the pixel’s state is “0”, no light from that pixel can contribute to the diffraction pattern of the device. Such a binary array is called a “genome” here, similar to the concept of “genome” in GA. In SHEA, before the evolutionary process begins, the large-pixelated metasurface containing  $M \times M$  pixels is first merged into a smaller pixelated metasurface with  $N \times N$  pixels. Here,  $M = nN$ , where  $n$  is a positive integer, for example,  $n = 2, 3, \dots$ . Hence, a “genome<sub>L</sub>” with  $N \times N$  superpixels can also be applied to represent the pixels’ states of the metasurface. Therefore, the original design task is reorganized into a segmented hierarchical task. The evolutionary process first begins from the lower segmentation where the metasurface pixels’ states are coarsely represented by “genome<sub>L</sub>”. Starting from a randomly generated initial “genome<sub>L</sub>”, the value of “genome<sub>L</sub>” will evolve through a mutation-only evolutionary process according to the evaluation of the fitness function. When the convergence conditions in the lower segmentations are satisfied, the optimized “genome<sub>L</sub>” will be sent to the higher segmentation, where an initial “genome<sub>H</sub>” (an  $M \times M$

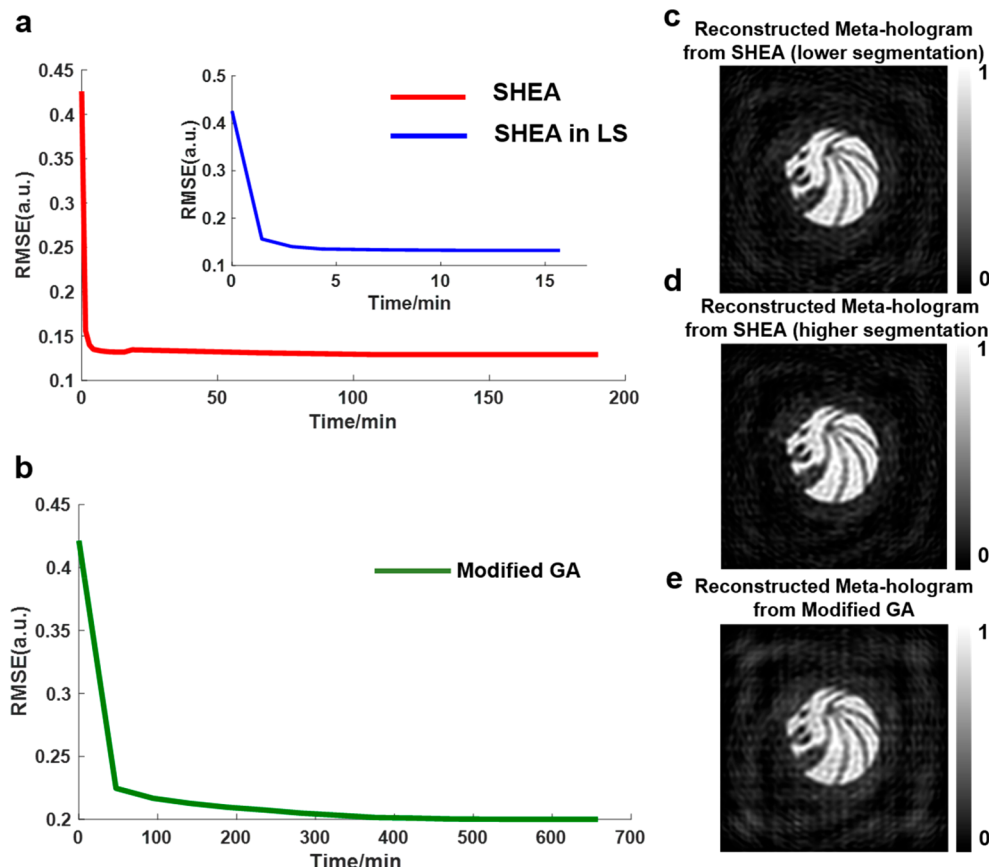


**Figure 2.** Comparison between SHEA and modified GA using RMSE as the fitness function. (a) RMSE as a function of computing time in SHEA. The inset picture in (a) shows RMSE as a function of computing time in SHEA in the lower segmentation (LS). (b) RMSE as a function of computing time in modified GA. (c) Simulated meta-hologram image reconstructed from the optimized genome<sub>L</sub> in lower segmentation of SHEA. (d) Simulated meta-hologram image reconstructed from the final optimized genome<sub>H</sub> in SHEA. (e) Simulated meta-hologram image reconstructed from the optimized genome in modified GA. Emblem used with permission from Seven Lions Music LLC.

array represents the pixels' states of the original metasurface) would be generated based on “genome<sub>L</sub>”, as shown in Figure 1a. Next, the mutation-only evolutionary process in the higher segmentation starts, and the final optimized “genome<sub>H</sub>” can be obtained after only several rounds of iterations. To illustrate the validity and easy implementation of SHEA, we design a broadband meta-hologram and full-color meta-holograms based on SHEA, as shown in Figure 1b. First, a broadband meta-hologram using SHEA is demonstrated. In order to show the details of the hologram image vividly, we target our design on a metasurface including a 302 × 302 pixel array, enabling  $2^{91204}$  possible combinations for the final solution. The period of each pixel on the metasurface is 300 nm × 300 nm; the incident light's wavelength is 532 nm, and the target plane is at  $z = 357 \mu\text{m}$  above the metasurface. Additionally, we also attempt to implement GA and modified GA to solve the same inverse design problem under the same implementation environment [Intel(R) Core (TM) i7-4770 CPU at 3.40 GHz, and 32 GB installed memory (RAM, random-access memory), Matlab 2015] to have a clear performance comparison among different algorithms.

During the evolutionary process, the employed fitness function has a crucial impact on both converging speed and final evolutionary result. RMSE (root-mean-square error) has been frequently employed as both the fitness function and performance evaluation criterion in previous binary-amplitude-controlled hologram designs. The RMSE can be expressed as

$$\text{RMSE} = \sqrt{\sum_{i=1,j=1}^{i=M,j=N} \frac{(I(i, j) - I_{\text{target}}(i, j))^2}{M \times N}} \quad (1)$$

where  $M$  is the total number of pixels along the  $x$  direction of the picture, and  $N$  is the number of total pixels along the  $y$  direction of the picture.  $I(i, j)$  denotes the intensity of the pixel  $(i, j)$  on the simulated diffraction pattern, whereas  $I_{\text{target}}(i, j)$  denotes the intensity of the pixel  $(i, j)$  on the original target image. As shown in eq 1, RMSE can provide the absolute difference between the original target image and the reconstructed image. A small RMSE means the reconstructed hologram has not only high fidelity but also good quality with high signal-to-noise ratio. Therefore, we first attempt to implement the three design paradigms (GA, modified GA, and SHEA) using RMSE as the fitness function to design the broadband meta-hologram. During the evolutionary process, the new generated genome, which can reconstruct images with smaller RMSE, will replace the old genome so that the reconstructed hologram image can gradually approach the original target.

During our efforts to implement the three design paradigms (GA, modified GA, and SHEA) for the large-pixelated meta-hologram, we find that the needed RAM using GA would exceed the RAM of a regular personal computer (32 GB) (detailed discussion is provided in the Supporting Information part 6). This is because, in GA, the initial population (the number of genomes) should be quite large for appropriately

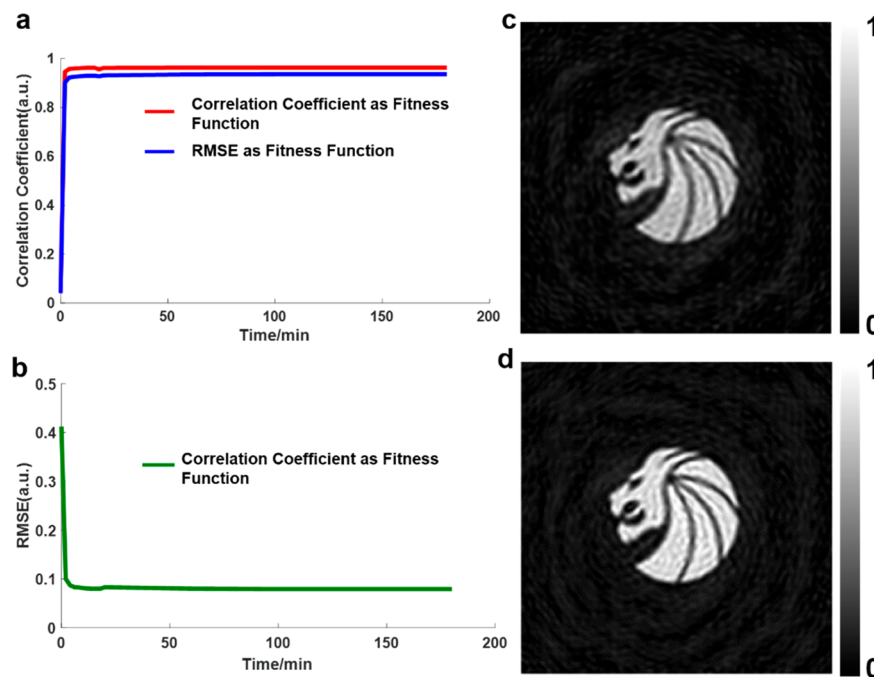


**Figure 3.** Performance comparison of SHEA with different fitness function. (a) CC as a function of computing time for SHEA with different fitness functions. The red solid line depicts the curve with CC as the fitness function, whereas the blue solid line depicts the curve with RMSE as the fitness function. (b) RMSE as a function of computing time for SHEA with CC as the fitness function. (c) Simulated metahologram image reconstructed from the genome<sub>L</sub> optimized in the lower segmentation of SHEA. (d) Simulated hologram image reconstructed from the final optimized genome<sub>H</sub> based on SHEA. Emblem used with permission from Seven Lions Music LLC.

solving this problem. To proceed with the selection, crossover, and mutation operations, the information on every genome in the population needs to be saved and sorted, which would take much computing time and space. Therefore, we infer that GA may not be suitable for solving large-pixelated complex inverse design on regular personal computers, and only modified GA and SHEA are implemented and compared. In SHEA, the size of genome<sub>L</sub> is chosen as  $151 \times 151$ , whereas the size of genome<sub>H</sub> is  $302 \times 302$ . Details of implementation using SHEA for this example is provided in part 1 of the *Supporting Information*. The performance comparison is provided in Figure 2.

Figure 2a,b shows how RMSE values change with computing time using SHEA and modified GA, respectively. The inset of Figure 2a shows how RMSE changes as a function of computing time using SHEA in lower segmentation (LS). As shown in Figure 2a,b, the RMSE values of the simulated results drop rapidly in both modified GA and SHEA at first, then the converging speeds slow down and finally the RMSE values reach stationary values. It is obvious that both algorithms are strictly monotonously converging to the final target. However, two major differences should be noted here. First, the converging speed of SHEA is tens of times faster than that of modified GA. In modified GA, it takes at least one round for the RMSE to drop from above 0.4 to below 0.25, and one round in modified GA takes around 47 min; however, in SHEA, it only takes one round in the lower segmentation to push the RMSE from above 0.4 to around 0.15, and the corresponding computing time only takes less than 2 min, as shown in the inset of Figure 2a. Second, the final result of SHEA is more optimized than that of modified GA. Due to the large array size, premature convergence may happen in modified GA, whereas in SHEA, due to the relatively smaller searching region in the lower segmentation, the mutation

operation in the lower segmentation can promote the genome pattern of the metasurface to quickly evolve into the “neighborhood” of the final optimum solution; then the mutation process in the higher segmentation will finely tune the result and approach the final optimized result. Therefore, SHEA can avoid premature convergence to some extent. To make the comparison rigorous enough, all the data summarized in Figure 2a,b are the average values of 100 runs using each algorithm. From Figure 2a, we find that the average final RMSE in this example using SHEA is around 0.13, whereas the one using modified GA is around 0.2, which also suggests that the converging ability of SHEA is stronger than that of modified GA when dealing with large data. Figure 2c shows the simulated reconstructed hologram image based on optimized genome<sub>L</sub> from the lower segmentation in SHEA. Figure 2d,e shows the simulated results of the reconstructed hologram images based on final optimized genome patterns from SHEA and modified GA, respectively. It is obvious that the reconstructed image from SHEA has a higher signal-to-noise ratio than that of modified GA.

From Figure 2c–e, we find that by using RMSE as the fitness function, performance balance among pixels of the image cannot be guaranteed. As a result, though the final optimized result may have an overall small error compared to the original target image, some singular pixels may still bear large differences compared to the target image, which would obviously impair the overall quality of the reconstructed image. The most straightforward outcome is that some spots on the generated image may be oversaturated, while some spots may be too dim. To overcome this, meanwhile seeking to explore even better optimization performance, we apply the correlation coefficient (CC) between the target image and the reconstructed image as the new fitness function to guarantee

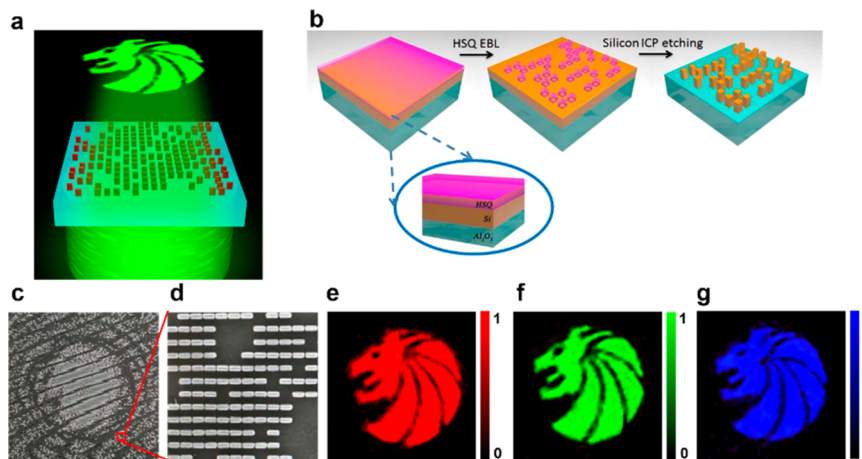


**Figure 4.** Experimental demonstration of the broadband meta-hologram designed by SHEA. (a) Sketch of the broadband Si hologram. Right-hand circularly polarized light is illuminated from the substrate side of the metasurface; left-hand circularly polarized light is collected from Si nanopillars to construct the hologram image. The reconstructed hologram image is floating above the metasurface at a focal distance at around 350  $\mu\text{m}$ . (b) Scheme of the nanofabrication process using EBL. (c) Overall SEM picture of the metasurface. (d) Zoomed-in SEM picture of part of the metasurface marked in (c). (e) Experimental result of broadband Si meta-hologram under 633 nm illumination. (f) Experimental result of broadband Si meta-hologram under 532 nm illumination. (g) Experimental result of broadband Si meta-hologram under 445 nm illumination. Emblem used with permission from Seven Lions Music LLC.

the overall behavior of our final result. Here, our new fitness function is defined as

$$F = \frac{E\{[T - E[T]][R - E[R]]\}}{\{E\{[T - E[T]]^2\}E\{[R - E[R]]^2\}\}^{1/2}} \quad (2)$$

where  $E[\cdot]$  is the expectation value and  $T$  and  $R$  denote the intensity profiles of the target image and reconstructed image, respectively. As is shown,  $F$  is actually the CC of the reconstructed image and the target image. During the evolutionary process, the genome which can generate larger CC would replace the old one, making  $F$  approach 1 gradually. Similar to the RMSE, the CC can also work as an analyzing criterion for the quality of the reconstructed image. Simulations using SHEA based on CC as the fitness function are carried out, as shown in Figure 3. Meanwhile, in order to have a valid comparison of optimization performances from all aspects, we employ both CC and RMSE as judging criteria to evaluate the quality of the reconstructed meta-hologram images built from different fitness functions. As shown in Figure 3, the converging speed of using CC in SHEA is even a bit faster than that of using RMSE. Figure 3a shows that the final CC when using CC as the fitness function is closer to 1 compared to using RMSE as the fitness function. Figure 3b shows the RMSE of the reconstructed images using CC as the fitness function. As shown in Figure 3b, within the first round in the lower segmentation, the RMSE drops from above 0.4 to around 0.1, and the final RMSE is around 0.08, which is much smaller than the previous optimized result using RMSE as the fitness function. Figure 3c,d show the reconstructed meta-hologram images based on optimized genome from the lower segmentation and higher segmentation using CC as fitness function. Comparing Figure 3d with Figure 2d, it is obvious that our established SHEA with CC as the fitness function can outperform previous one from all aspects. To make our conclusion valid, all the data in Figure 3a,b are the average values summarized from 100 runs.

To further validate the performance of our SHEA, more experimental demonstrations were carried out. When designing binary-amplitude-controlled meta-optics devices, the nanohole

structure always comes first in our mind due to its simple design and easy fabrication. However, the transmission efficiency of the nanohole structure is low, and the transmission spectrum of light highly depends on the periodicity of the nanoholes. This would impair the effect of the meta-holograms, such as resolution, efficiency, and so on (detailed discussion is provided in the Supporting Information part 2). Therefore, silicon (c-Si) is chosen here for its high refractive index in the visible regime, which enables the tuning of high-quality electric/magnetic resonances confined in the Si nanostructures.<sup>25–28</sup> Meanwhile, its low cost, mature fabrication technology, and good compatibility with CMOS technology provide its potential in real-life applications.

We first implemented a broadband hologram on a subwavelength pixelated metasurface covering from 445 to 633 nm. The metasurface is composed of judiciously designed Si nanopillars arranged aperiodically on a sapphire substrate, as shown in Figure 4a. A circularly polarized light is normally incident from the substrate side of the metasurface. Each Si nanopillar works as a broadband half-wave plate with high conversion efficiency in the visible regime in the transmission mode. Here, the conversion efficiency is defined as

$$\eta = \frac{T_{\text{opp}}}{T_{\text{total}}} \times 100\% \quad (3)$$

where  $T_{\text{opp}}$  denotes the energy of the transmitted light with opposite handedness polarization of the incident light, and  $T_{\text{total}}$  denotes the energy of the total transmitted light. To enable the meta-hologram to work in a broadband region, the dimensions of the Si nanopillar are optimized so that the conversion efficiency of the Si nanopillar over the whole visible spectrum can be as high as possible. Here, the dimensions of the Si nanopillar are chosen as 80 nm  $\times$  250 nm  $\times$  300 nm, whereas the periods of each pixel are 300 nm  $\times$  300 nm. Simulated conversion efficiencies for 633, 532, and 445 nm are 42.6%, 27.4%, and 26.7%, respectively. For the total efficiency of the meta-hologram, we did not simulate the overall metasurface consisting of aperiodically distributed nanopillars due to our limited computational source. Considering our

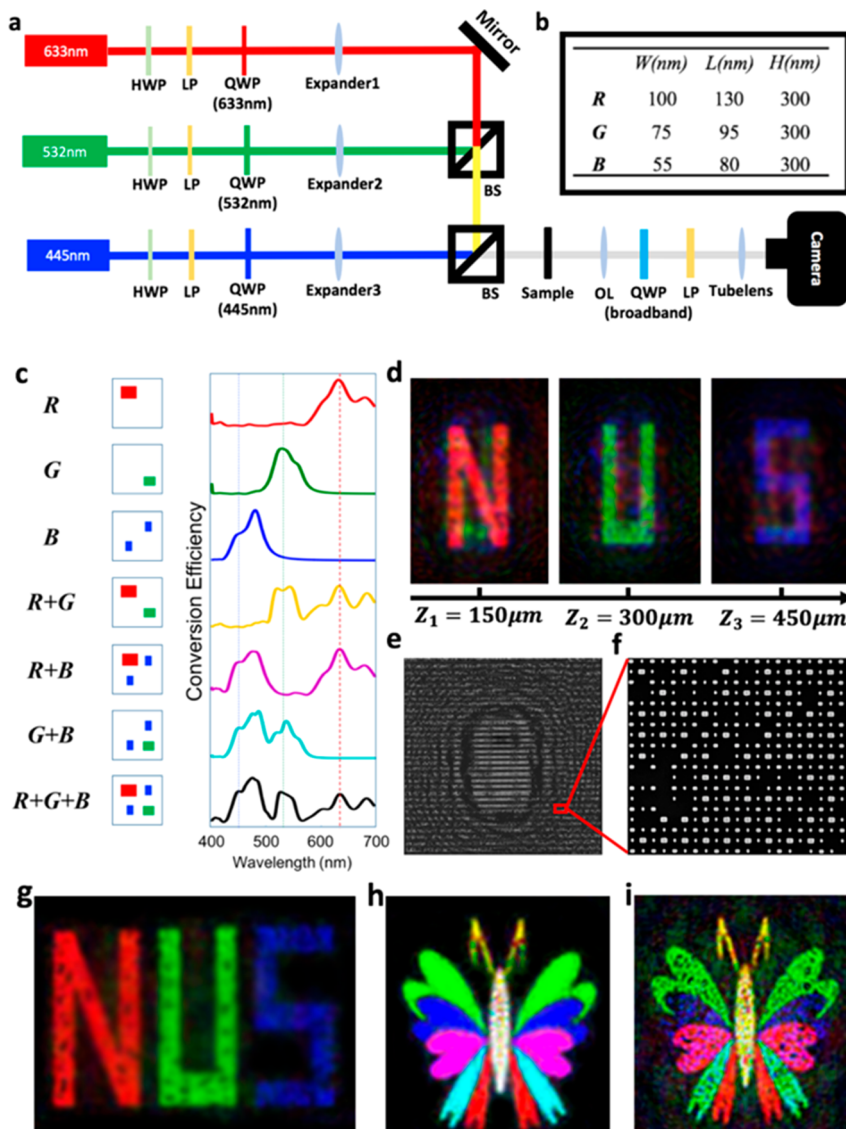


**Figure 5.** Experimental demonstration of the full-color meta-holograms designed by SHEA. (a) Experimental setup of full-color meta-hologram. HWP, half-wave plate; LP, linear polarizer; QWP, quarter-wave plate; BS, beam splitter. Three expanders are applied to adjust the beam sizes from three lasers into uniform size. (b) Dimensions of three Si nanopillars for red (R), green (G), and blue (B) light conversion. (c) Conversion efficiencies of seven supercells containing different combinations of nanopillars. (d) Experimental results of the reconstructed on-axis “N”, “U”, and “S” images. (e) SEM picture of the overall on-axis NUS sample. (f) SEM picture of a small part of the sample in (e). (g) Experimental result of reconstructed “NUS” image. (h) Simulation result of reconstructed full-color butterfly. (i) Experimental result of reconstructed full-color butterfly image.

available computational source, we simulated the total efficiency of a smaller version metasurface containing  $101 \times 101$  pixels but with similar filling ratio of the fabricated sample as an estimation. Here, the filling ratio is denoted by the total number of silicon nanopillars on the metasurface over the total pixel number of the metasurface, and the simulated overall efficiencies for the  $101 \times 101$  pixelated metasurface at 633, 532, and 445 nm are 15.7%, 10.8%, and 9.6%, respectively. Figure 4b shows the fabrication process of the silicon meta-hologram. The metasurface is fabricated on a commercially available 300 nm thick c-Si(100) epitaxially grown on a sapphire substrate (from UniversityWafer, Inc.). The structure was patterned on a negative resist (hydrogen silsesquioxane, HSQ) using an E-beam writer (Raith E-line, 30 kV). After developing the resist, we transferred the pattern from the resist into the silicon layer using inductively coupled plasma etching

(PlasmaPro System 100ICP180). Finally, the remaining HSQ was removed with hydrofluoric acid. Scanning electron microscopy (SEM) pictures of the sample are shown in Figure 4d,e, and the experimental setup is depicted in Figure S2. Because the hologram is originally designed at a focal distance of 357  $\mu\text{m}$  at 532 nm working wavelength, according to Fresnel’s principle, the reconstructed meta-hologram should also appear at around 300  $\mu\text{m}$  and 427  $\mu\text{m}$  when we change the illuminating light to be 633 nm and 445 nm lasers, respectively. The measured results for the broadband silicon meta-hologram are shown in Figure 4e–g. The distortions between the simulated image and the measured image may be attributed to imperfect fabrication of the sample, and the measured total efficiencies of the broadband Si hologram are 14.87%, 9.86%, and 8.68% at 633 nm, 532 nm, and 445 nm, respectively.

Full-color meta-hologram has been one of the most interesting topics in metasurfaces due to its vivid holographic imaging and large data storage ability at a small size. Such techniques can be widely applied in high-ranking information security, encryption, and decoding, such as personal identification card, commodity tags, and so on. One of the most critical problems in full-color meta-holograms is the crosstalk among different colors which would impair the fidelity of the reconstructed hologram. In addition, many reported meta-holograms so far are built on an off-axis scheme, making it inconvenient for integration and packaging in practical life applications. In this work, we designed three full-color meta-holograms in the on-axis transmission mode which have overcome the aforementioned two problems. To eliminate the crosstalk between different colors, a supercell containing three different kinds of silicon nanopillars with different sizes are carefully designed. The detailed dimensions of the three Si nanopillars are listed in Figure 5b. The dimension of the subwavelength supercell is 400 nm × 400 nm. To apply the SHEA for the full-color meta-hologram designs, we first obtain the red (R), green (G), and blue (B) components of the target images. Then, the SHEA is implemented three times to optimize the genome patterns for the R, G, and B components of the target images for each hologram. According to the evolutionary results from SHEA, there should be seven different combinations of Si nanopillars contained in a supercell, as listed in Figure 5c. Those seven combinations guarantee the seven distinct color generations of red, green, blue, yellow, magenta, cyan, and white. Through tailored designing of the structures, in each supercell, the conversion efficiency of the desired color is almost 20 times the conversion efficiency of the undesired ones, thus strictly eliminating the crosstalk effect (detailed conversion efficiencies for all cases listed in Figure 5c are provided in part 4 of the Supporting Information). Meanwhile, the conversion efficiencies of the three original colors (RGB) are kept relatively in balance with each other, ensuring good quality of the full-color images.

The experimental results of the full-color meta-holograms are shown in Figure 5d,g,i. In Figure 5d, we showed the reconstructed images of an achromatic meta-hologram which distributed images composed of different wavelengths to different focal planes. As shown in Figure 5d, a red "N", a green "U", and a blue "S" emerge above the metasurface at a distance of around 150 μm, 300 μm, and 450 μm, respectively. The crosstalk between different letters is caused by their on-axis arrangement rather than structure spectrum crosstalk, and the measured total efficiencies for the "N", "U", and "S" are 7.94%, 7.83%, and 5.62%, respectively. Apart from this, a meta-hologram which shows "NUS" with three original colors (RGB) floating above the meta-hologram surface at a distance of 400 μm is also designed. As shown in Figure 5g, three letters with different colors are captured on the same focal plane with almost zero crosstalk, which clearly demonstrates the performance of crosstalk-eliminated nanopillars. Meanwhile, the experimental results clearly show the edges of the letters, confirming the validation of our algorithm. The measured total efficiencies for the red, green, and blue components are 6.54%, 7.27%, and 4.89%, respectively. The above experimental results clearly demonstrate that our meta-holograms can explicitly control the dispersion of visible light both in the vertical direction and in the horizontal direction, fulfilling the full control of the dispersion of visible light. Finally, a full-color meta-hologram which contains not only the three original

colors (RGB) but also their secondary colors (cyan, magenta, and yellow) and third color (white) is designed and measured. Figure 5h shows the simulation result of the full-color butterfly. The body of the butterfly is white, the tentacles of the butterfly are yellow, and the colorful wings of the butterfly contain five different colors, which are green, blue, magenta, cyan, and red from top to bottom. The corresponding experimental result is shown in Figure 5i, and the corresponding total efficiencies for the red, green, and blue components are 6.12%, 7.67%, and 4.05%, respectively. We notice that there are some "black dots" in the experimental reconstructed image, and the shape of the butterfly wings are slightly distorted from the simulated result. Again, these differences mostly arise from the imperfection fabrication. Because the sizes of the nanopillars are quite small, especially the one which emits blue light, the fabrication is quite challenging.

## CONCLUSIONS

In conclusion, we proposed a design paradigm based on SHEA to solve amplitude-controlled complex inverse meta-optics designs. The SHEA is proven to be able to solve complex meta-optics design tasks, which contain large amounts of variables at a rapid converging speed. Meanwhile, we proposed an improved fitness function based on CC that may greatly improve the final evolutionary result. Based on these, a broadband silicon meta-hologram is designed and three full-color meta-holograms with only amplitude control are also demonstrated in this work as typical proof-of-concept examples. The experimental results of the holograms proved the validation of SHEA. This design paradigm can not only be applied in hologram designs but also be employed in the inverse design of various complex near-field/far-field meta-optics devices when coupled with proper theoretical models. Our proposed SHEA and improved fitness function can find important applications in the design of future high-quality and even multi-objective meta-optics devices.

## METHODS

**Numerical Simulation.** In this work, the design of the Si nanopillars in the metasurface was conducted using Lumerical (FDTD Solution). In this simulation, periodic boundary conditions were applied along the *x* and *y* directions, and perfect matched layer boundary conditions were applied along the *z* direction, that is, light's propagation direction. The measured dielectric constant of Si was used in the simulation.

**Fabrication.** The metasurface was fabricated on a commercially available 300 nm thick c-Si(100) epitaxially grown on a sapphire substrate (from UniversityWafer, Inc.). The structure was patterned on a negative resist (HSQ) using an E-beam writer (Raith E-line, 30 kV). After developing the resist, we transferred the pattern from the resist into the silicon layer using inductively coupled plasma etching (PlasmaPro System 100ICP180). The remaining HSQ was removed with hydrofluoric acid.

## ASSOCIATED CONTENT

### Supporting Information

The Supporting Information is available free of charge on the ACS Publications website at DOI: 10.1021/acsnano.8b08333.

Implementation of SHEA for the broadband Si hologram, discussion of using nanohole structures for full-color meta-hologram, experimental setup for measuring the broadband meta-hologram, detailed conversion efficiencies of Si nanopillars designed for full-color meta-holograms, discussion on applying SHEA for

phase-controlled optical devices, discussion on absence of comparison between GA and SHEA ([PDF](#))

## AUTHOR INFORMATION

### Corresponding Authors

\*E-mail: [shumin.xiao@hit.edu.cn](mailto:shumin.xiao@hit.edu.cn).

\*E-mail: [chengwei.qiu@nus.edu.sg](mailto:chengwei.qiu@nus.edu.sg).

### ORCID

Joel K. W. Yang: [0000-0003-3301-1040](#)

Shumin Xiao: [0000-0002-0751-9556](#)

Cheng-Wei Qiu: [0000-0002-6605-500X](#)

### Author Contributions

•Z.J., S.M., S.C., and Y.L. contributed equally to this work. Z.J., S.M., S.C., Y.L., and C.-W.Q. conceived the idea; Z.J. and S.M. performed the experiments; S.C., Y.L., and Y.H. supported the experiments; S.X. and C.Z. did the nano-fabrication of the metasurface. X.Y., C.Y., J.K.W.Y., and B.L. participated in the discussions and provided valuable suggestions. The paper was drafted by Z.J. with input from C.Z., S.M., S.X., and C.-W.Q. All authors analyzed the data, read, and corrected the manuscript before the manuscript submission. C.-W.Q. and S.X. supervised the project.

### Notes

The authors declare no competing financial interest.

## ACKNOWLEDGMENTS

C.-W.Q. acknowledges the financial support from the National Research Foundation, Prime Minister's Office, Singapore under its Competitive Research Program (CRP award NRF-CRP15-2015-03). S.X. would like to thank the Shenzhen Fundamental research project for financial support (Grant No. JCYJ20160505175637639). S.C. would like to thank the Guangdong Natural Science Foundation for financial support (Grant No. 2016A030310065), Science and Technology Planning Project of Guangdong Province (2016B050501005). Y.L. would like to thank the National Natural Science Foundation of China for financial support (Grant No. 61575127). Z.J. would like to give special thanks to Seven Lions music for their company during these years and for their generous permission to allow us to use their logo image in our meta-hologram design.

## REFERENCES

- (1) Wan, W.; Gao, J.; Yang, X. Full-Color Plasmonic Metasurface Holograms. *ACS Nano* **2016**, *10*, 10671–10680.
- (2) Kruk, S.; Kivshar, Y. Functional Meta-Optics and Nanophotonics Govern by Mie Resonances. *ACS Photonics* **2017**, *4*, 2638–2649.
- (3) Kivshar, Y. All-Dielectric Meta-Optics and Non-Linear Nanophotonics. *Natl. Sci. Rev.* **2018**, *5*, 144–158.
- (4) Mei, S.; Mehmood, M. Q.; Hussain, S.; Huang, K.; Ling, X.; Siew, S. Y.; Liu, H.; Teng, J.; Danner, A.; Qiu, C.-W. Flat Helical Nanosieves. *Adv. Funct. Mater.* **2016**, *26*, 5255–5262.
- (5) Sun, S.; Zhou, Z.; Zhang, C.; Gao, Y.; Duan, Z.; Xiao, S.; Song, Q. All-Dielectric Full-Color Printing with TiO<sub>2</sub>Metasurfaces. *ACS Nano* **2017**, *11*, 4445–4452.
- (6) Dong, Z.; Ho, J.; Yu, Y. F.; Fu, Y. H.; Paniagua-Dominguez, R.; Wang, S.; Kuznetsov, A. I.; Yang, J. K. W. Printing Beyond sRGB Color Gamut by Mimicking Silicon Nanostructures in Free-Space. *Nano Lett.* **2017**, *17*, 7620–7628.
- (7) Hu, J.; Liu, C.-H.; Ren, X.; Lauhon, L. J.; Odom, T. W. Plasmonic Lattice Lenses for Multiwavelength Achromatic Focusing. *ACS Nano* **2016**, *10*, 10275–10282.
- (8) Huntington, M. D.; Lauhon, L. J.; Odom, T. W. Subwavelength Lattice Optics by Evolutionary Design. *Nano Lett.* **2014**, *14*, 7195–7200.
- (9) Wang, B.; Dong, F.; Li, Q.-T.; Yang, D.; Sun, C.; Chen, J.; Song, Z.; Xu, L.; Chu, W.; Xiao, Y.-F.; Gong, Q.; Li, Y. Visible-Frequency Dielectric Metasurfaces for Multiwavelength Achromatic and Highly Dispersive Holograms. *Nano Lett.* **2016**, *16*, 5235–5240.
- (10) Zhang, L.; Mei, S.; Huang, K.; Qiu, C.-W. Advances in Full Control of Electromagnetic Waves with Metasurfaces. *Adv. Opt. Mater.* **2016**, *4*, 818–833.
- (11) Yoon, G.; Lee, D.; Nam, K. T.; Rho, J. "Crypto-Display" in Dual-Mode Metasurfaces by Simultaneous Control of Phase and Spectral Responses. *ACS Nano* **2018**, *12*, 6421.
- (12) Li, Z.; Kim, I.; Zhang, L.; Mehmood, M. Q.; Anwar, M. S.; Saleem, M.; Lee, D.; Nam, K. T.; Zhang, S.; Luk'yanchuk, B.; Wang, Y.; Zheng, G.; Rho, J.; Qiu, C.-W. Dielectric Meta-Holograms Enabled with Dual Magnetic Resonances in Visible Light. *ACS Nano* **2017**, *11*, 9382–9389.
- (13) Huang, K.; Dong, Z.; Mei, S.; Zhang, L.; Liu, Y.; Liu, H.; Zhu, H.; Teng, J.; Luk'yanchuk, B.; Yang, J. K. W.; Qiu, C.-W. Silicon Multi-Meta-Holograms for the Broadband Visible Light. *Laser Photonics Rev.* **2016**, *10*, 500–509.
- (14) Jin, L.; Dong, Z.; Mei, S.; Yu, Y. F.; Wei, Z.; Pan, Z.; Rezaei, S. D.; Li, X.; Kuznetsov, A. I.; Kivshar, Y. S.; Yang, J. K. W.; Qiu, C.-W. Noninterleaved Metasurface for (261) Spin-and Wavelength-Encoded Holograms. *Nano Lett.* **2018**, *18* (12), 8016–8024.
- (15) Shen, B.; Wang, P.; Polson, R.; Menon, R. An Integrated-Nanophotonics Polarization Beamsplitter with 2.4 × 2.4 μm<sup>2</sup> Footprint. *Nat. Photonics* **2015**, *9*, 378.
- (16) Piggott, A. Y.; Lu, J.; Lagoudakis, K. G.; Petykiewicz, J.; Babinec, T. M.; Vučković, J. Inverse Design and Demonstration of a Compact and Broadband On-Chip Wavelength Demultiplexer. *Nat. Photonics* **2015**, *9*, 374.
- (17) Wiecha, P. R.; Arbovet, A.; Girard, C.; Lecestre, A.; Larrieu, G.; Paillard, V. Evolutionary Multi-Objective Optimization of Colour Pixels Based on Dielectric Nanoantennas. *Nat. Nanotechnol.* **2016**, *12*, 163.
- (18) Forestiere, C.; He, Y.; Wang, R.; Kirby, R. M.; Dal Negro, L. Inverse Design of Metal Nanoparticles' Morphology. *ACS Photonics* **2016**, *3*, 68–78.
- (19) Weile, D. S.; Michielssen, E. Genetic Algorithm Optimization Applied to Electromagnetics: A Review. *IEEE Trans. Antennas Propag.* **1997**, *45*, 343–353.
- (20) Jiang, Z. H.; Yun, S.; Toor, F.; Werner, D. H.; Mayer, T. S. Conformal Dual-Band Near-Perfectly Absorbing Mid-Infrared Metamaterial Coating. *ACS Nano* **2011**, *5*, 4641–4647.
- (21) Egorov, V.; Eitan, M.; Scheuer, J. Genetically Optimized All-Dielectric Metasurfaces. *Opt. Express* **2017**, *25*, 2583–2593.
- (22) Hu, J.; Ren, X.; Reed, A. N.; Reese, T.; Rhee, D.; Howe, B.; Lauhon, L. J.; Urbas, A. M.; Odom, T. W. Evolutionary Design and Prototyping of Single Crystalline Titanium Nitride Lattice Optics. *ACS Photonics* **2017**, *4*, 606–612.
- (23) Fu, P.-H.; Lo, S.-C.; Tsai, P.-C.; Lee, K.-L.; Wei, P.-K. Optimization for Gold Nanostructure-Based Surface Plasmon Biosensors Using a Microgenetic Algorithm. *ACS Photonics* **2018**, *5*, 2320–2327.
- (24) Wu, Y.; Cao, S.; Hua, L.; Zhao, D. Design and Demonstration of A New Kind of Aperture for Getting Expected Diffraction Patterns. *Opt. Lett.* **2014**, *39*, 801–804.
- (25) Wang, Y.; Zhang, N.; Jiang, Z.; Wang, L.; Xiao, Y.; Sun, W.; Yi, N.; Liu, S.; Gu, X.; Xiao, S.; Song, Q. Chip-Scale Mass Manufacturable High-Q Silicon Microdisks. *Adv. Mater. Technol.* **2017**, *2*, 1600299.
- (26) Zhang, N.; Gu, Z.; Liu, S.; Wang, Y.; Wang, S.; Duan, Z.; Sun, W.; Xiao, Y.-F.; Xiao, S.; Song, Q. Far-field Single Nanoparticle Detection and Sizing. *Optica* **2017**, *4*, 1151–1156.
- (27) Wang, L.; Zhang, S.-X.; Song, Q.; Gong, Q.; Xiao, Y.-F. Light Confinement in A Low-Refraction-Index Microcavity Bonded on A Silicon Substrate. *Optica* **2016**, *3*, 937–940.

- (28) Zhang, X.; Cao, Q.; Wang, Z.; Liu, Y.; Qiu, C.; Yang, L.; Gong, Q.; Xiao, Y. Symmetry-Breaking-Induced Nonlinear Optics at a Microcavity Surface. *Nat. Photonics* **2019**, *13*, 21–24.